High frequency characterization of a sweeping jet actuator

Célestin Ott, Quentin Gallas, Jérôme Delva, Marc Lippert, Laurent Keirsbulck

High Frequency Characterization of a Sweeping jet Actuator

C. Ott[a,b], Q. Gallas[a], J. Delva[a], M. Lippert[b], L. Keirsbulck[b]

[a]Cnrs, Onera, *Centrale Lille, Univ. Lille, Arts et Métiers ParisTech, Laboratoire de Mécanique des Fluides de Lille - Kampé de Fériet (*Lmfl*), F-59000, Lille, France*
[b]Lamih, Umr Cnrs 8201, *Le Mont Houy, 59313 Valenciennes, France*

Sweeping jets are an emerging type of actuators that have gained interest due to their potential use in flow control applications. The working principle of these devices is based on the bi-stable attachment of a jet to adjacent walls. They are able to produce unsteady blowing within a wide range of operating frequencies. Nevertheless, the state of art shows a lack of space-time characterization of these actuators for high sweeping frequencies. This paper resents a conditional approach that reconstructs the spatial dynamic response of sweeping jets for sweeping frequencies above 500 Hz. The time-dependent velocity is measured with two single-hot-wire sensors: a reference one placed at the edge of the exit nozzle, and a flying one. The method is then tested to characterize the flow at the exit nozzle of an in-house sweeping jet actuator with $1mm$ space resolution, and 50 μs time resolution. These measurements are performed with a sweeping frequency of 639 Hz. Overall this paper demonstrates that the conditional approach is very useful for understanding the physics of flow control actuators.

Keywords: Flow control; Sweeping Jet; Sychronized Hot-Wire; Conditional Approach; Dynamic Characterization.

1. Introduction

Active flow control is the ability to manipulate a flow field in order to improve the efficiency or performance of a fluidic system [1]. Flow control is of great technological interest and constitutes a leading area of research for scientists and engineers in fluid mechanics. Active flow control generally uses actuators to inject energy in the flowb(to amplify instabilities or to increase the boundary layer robustness for instance). Conventionally, these actuators can be turned on and off during an experiment, and some settings can be adjusted (frequency, amplitude ...). It is currently a growing field, thanks to the recent improvements of the fluid mechanics' scientific community's understanding. Active flow control can be divided into two main strategies. The first one aims to affect the flow behavior using high amplitude "brute-force" control. The second flow control strategy is based on the injection of small-amplitude perturbations into the flow to amplify the flow instabilities. The latter approach provides the advantage of reducing the power, size, and mass of the actuators ([1],[2],[3],[4],[5]). Resulting in lower power consumption, faster response, more reliability, and lower cost [6], which are desired characteristics for flow control actuators.

Among the various existing control devices, sweeping jets are an emerging type of actuators with the particularity of working without energetic inputs and being very robust. They started to be developed in the late 1970s at Harry Diamond Research Laboratories where they were initially considered to be used in analog computers and as a fluidic amplifier ([7],[8]). For years they have been mostly used with water as working fluid (as oscillating windshield washers on cars, showerheads and irrigation systems). These actuators have recently gained interest as controllers thanks to their simple and robust design, as well as their wide range of use concerning flow conditions ([9],[10],[11][12],[13],[14],[15],[16],[17],[18]). To design an efficient control strategy, the knowledge of the actuator dynamic response is critical and requires appropriate characterization to understand the jet topology, to quantify the homogeneity and the amplitude responses (concerning velocity, frequency, RMS ...). The range of sweeping frequency of the actuators is quite wide (from 10 Hz to 25 kHz [19]). Fig.1 shows the frequency and velocity ranges of some sweeping jet actuators studied in the state of art.

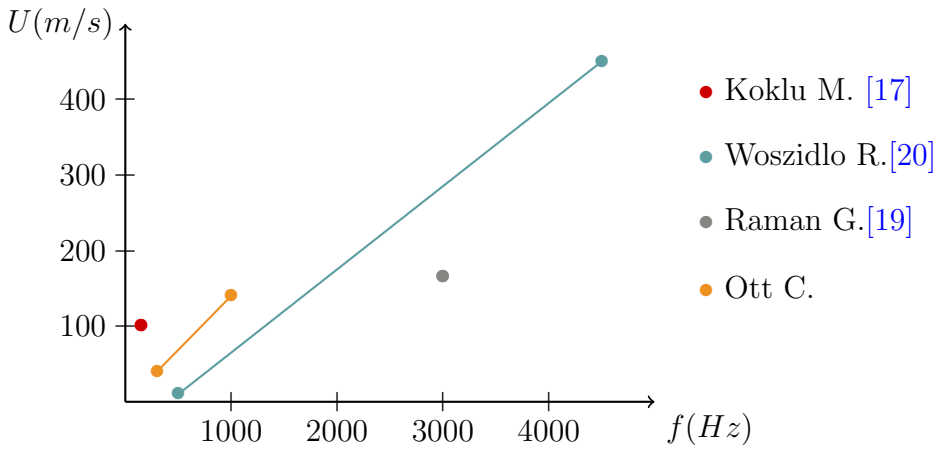

Figure 1 – Sweeping Jet Actuator Response in the State of Art.

The literature gives numerous characterization methods such as local time-resolved at high sweeping frequency ([8],[19],[20],[21]), spatially-resolved snapshots ([22]), space-time resolved at low sweeping frequency ([23],[22],[24]), numerical analysis and simulations ([25],[26],[27],[28]). Since the flow control actuation by sweeping jet is relatively recent [29], the state of art shows a lack of characterization process in order to correctly define the high frequency dynamic response. For this reason, a conditional approach based on a synchronization methodology is presented and tested on a particular operating point of a sweeping jet actuator. This requires first a full characterization of the sweeping jet actuator. The present paper is arranged as follows: first, the design and principle of the in-house sweeping jet are described in section 2. Then the synchronization methodology used to obtain a space-resolved and time-resolved characterization and the experimental setups used to characterize this actuator at the ONERA Lille are presented in section 3. These measurements, involving shadowgraph visualizations and single-wire hot-wire measurements, are used to obtain a baseline flow field characterization, which is reported in section 4. It leads to the

particular operating point of interest (639 Hz) and an apropriate setup (sensors locations) to test the synchronization methodology. This characterization is achieved by using two single-hot-wire sensors, including one that is scanning the interest zone. The method is used to describe characterize the flow at the exit nozzle of the actuator at high sweeping frequencies. The results of this dynamical response of the in-house actuator are introduced in section 5. In the present paper the superscript $*$ denotes the dimensionless parameters by h, the sweeping jet length, T, the sweeping period and U_{MAX} the maximum velocity.

2. Device Principle and Design

This section presents the sweeping jet actuator principle and the specific configuration that is developed in this paper. Sweeping jet actuators are attractive because they do not need an energetic controller to work and do not contain any moving parts. This type of actuator generates an oscillating jet when continuously supplied with pressurized air. From a flow control point of view, the working process of this actuator can be assimilated to the steady blowing, although it uses less air ([30],[31]). The actuator blows a continuous jet that oscillates from one side of the outlet nozzle to the other. Fig.2(a) shows the conventional design of a sweeping jet actuator, made of: an air input A, where the inlet pressure and mass flow is controlled, a main channel B, two feedback channels C that are propagating an over-pressure or a pressure drop from the outlet to the inlet, and an outlet nozzle D. The principle of the sweeping jet is the following : after switching on the steady air supply, the air flows through the actuator main cavity and attaches to either side of the cavity due to Coanda effect (Fig.2(b)). A backflow develops in the feedback channel and forces the jet flow separation from that surface and the reattachment to the opposite surface (Fig.2(c)). Then backflow also develops in the other feedback channel (Fig.2(d)) which forces the jet to switch back to its initial state (Fig.2(e)). The process then repeats, thus producing a self-sustaining oscillation process.

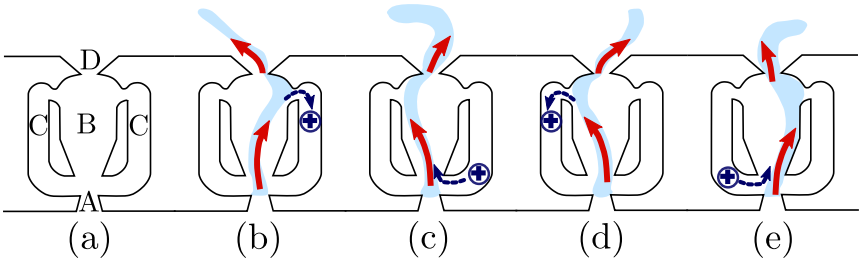

Figure 2 – Sweeping Jet: principle
Cross symbol denotes the high pressure region.

The sweeping frequency and velocity of the jet depends on the inlet pressure and the flow rate passing through the inlet nozzle. The only way to modify the actuator behavior is to modify its geometry (for instance the feedback channel size to modify the frequency or the

inlet and outlet nozzle for the velocity). The design of the in-house sweeping jet actuator studied is based on the work of I. Wygnanski et al.([32],[33]). The actuator was validated for inflight flow control uses during a flight test campain to increas the side force on an aircraft vertical tail [29]. The actuator geometrical proportions are conserved ([20]). However, the actuator is scaled up to provide an exit nozzle of 25 $mm \times 2.5\ mm$ and feedback channels of about 12 mm long. As shown further in this article, this geometry allows to have a wide range of outlet velocities (from 40 $m.s^{-1}$ to 140 $m.s^{-1}$) and sweeping frequency (300 Hz to 1 kHz) for a narrow inlet pressure range (from 0.5 bar to 4.5 bar). For further experiments (sweeping jet in crossflow), the actuator is integrated into an enclosure with a 45° inclined jet. This angle is chosen with the expectation of an efficient flow control actuator in the flat plate boundary layer configuration (intended in further experimentation). Fig.3 shows a schematic of the main geometric characteristics of the fluidic device used in the present work. This actuator is manufactured using resin stereolithography (which is a cost effective, robust and accurate manufacturing process in this case and at this scale).

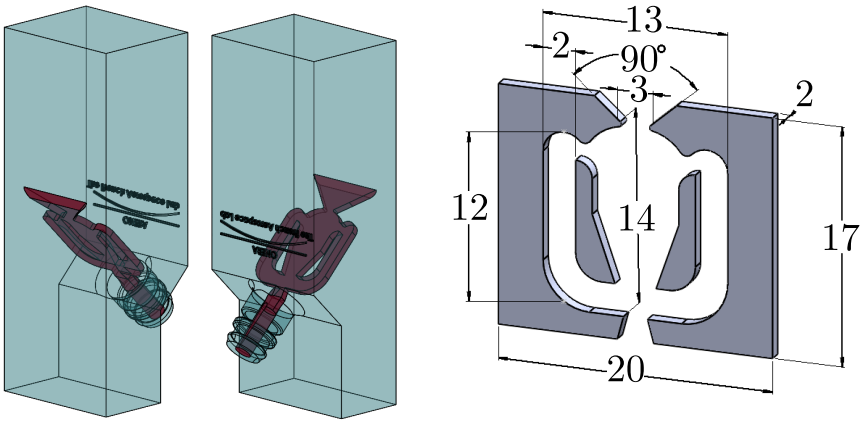

Figure 3 – In-house sweeping jet actuator design.
Lengths are in mm on the diagram.

3. Experimental Setup

The sweeping jet actuators presented in the previous section is characterized using different techniques. The shadowgraph technique provides qualitative results in order to assess the main structure of the jet. The time-resolved velocity flow field is also measured with a single hot wire probe. This section presents these techniques and the post-processing methodology developed to convert local time-resolved signal into spatially-resolved snapshots.

3.1. Shadowgraph Technique

The shadowgraph bench at ONERA Lille uses a mirror system to visualize the second derivative of the density field. 24 high-resolution cameras are deployed to acquire the shadowgraph visualizations. The bench (Fig.4) is made of two parabolic mirrors with a focal

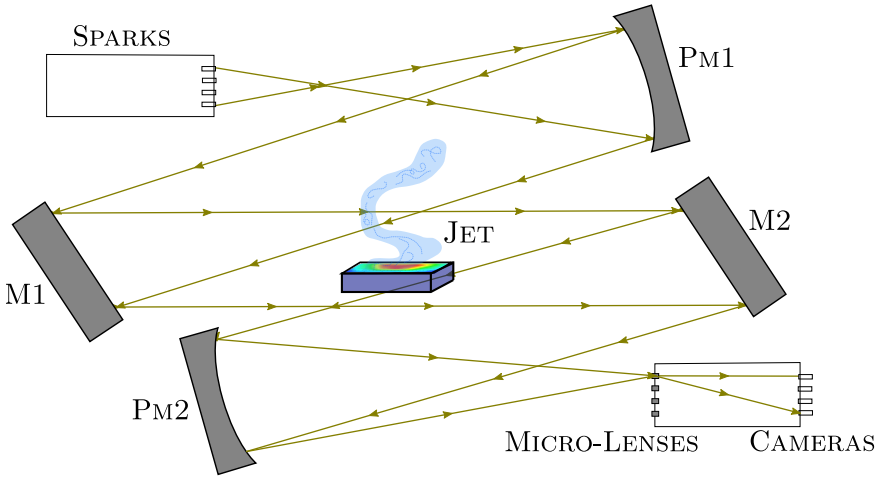

Figure 4 – Shadowgraph Setup

length of $f = 3.73\ m$ and a diameter of 400 mm (Pm1 and Pm2), two plan mirrors (M1 and M2) and a grid of 24 micro-lenses (focal length of $f = 20\ mm$). The format of the micro-lenses grid is 4 in X direction $\times$ 6 in the Y direction. The spacing between two lenses is 33.8 mm in the X direction and 31 mm in the Y direction. 24 Cranz-Schardin high voltage sparks are used as light sources. The light beams are collimated by the first parabolic mirror Pm1, then reflected by the first plan mirror M1 and finally deviated by the varying refractive index in the jet. The parallel light is then refocused by a second parabolic mirror Pm2, reflected by the second plan mirror M2, and redistributed to each cameras thanks to micro-lenses. This setup is used to visualize the jet envelop on two perpendicular plans defined on Fig.5.

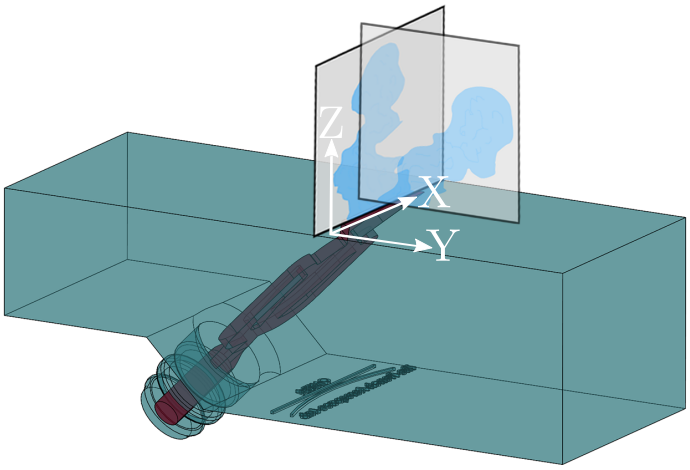

Figure 5 – Spatial System Coordinates

3.2. Hot-Wire Measurements

The hot-wire characterization is performed on the actuators test bench at ONERA Lille ([12]). The bench is equipped with a 6 *bar* air supply, a Sentronics proportional valve that regulates the pressure with a precision of 0.01 *bar* measured and regulated approximately 40 *cm* upwind the actuator inlet nozzle, inside the supply pipe, and a motorized arm with stepping motors to move the hot-wire with an accuracy of 0.1 *mm* in all directions. DANTEC Dynamics single-hot-wire probe type 55P15 and 55R01 (operating at constant temperature) connected to a DANTEC Dynamics conditioner (featuring a Wheatstone bridge and a low pass filter with a cutting frequency of 10kHz) are employed to survey the velocity response of the actuator at its outlet nozzle. The velocity measurements are sampled at $20kHz$ and the test duration is chosen to be equal to $4s$ (corresponding to more than 3000 sweeping jet periods). Since the velocity measured is under 100 m/s, the compressibility effect on hot-wire measurement are considered as insubstantial. The sensor is calibrated between 0 m/s and 150 m/s. The uncertainty is obtained from the calibration unit and can be evaluated to be less than 0.5 m/s for the present measured velocity range.

3.3. Hot-Wire Synchronization Methodology

In order to perform a conditional analysis, a stationary hot-wire sensor is used as a reference for the time synchronization of the two hot-wire sensors. This reference hot-wire, placed at the left-hand edge of the exit nozzle, used to identify the velocity peaks corresponding to the sweeping periods. The position of this sensor is critical: on one hand, the sensor has to be close enough to the jet in order to capture every period. On the other hand, it has to be placed at the edge of the jet to capture only one peak per period and to minimize the impact of the sensor on the jet development. In fact, the reference hot-wire being upstream the traveling hot-wire, the intrusiveness of the sensor is a substantial factor. The optimal position of the probe is found with an iterative process based on a trial and error approach. The final position is at 1 *mm* downwind the exit nozzle, and at 2 *mm* from the exit nozzle in the span direction. The peaks measured with the reference sensor are used to synchronize the time references between the two sensors with a conditional approach: the peaks are used as triggers. The second hot-wire sensor is mounted on a traverse system which scans the exit nozzle of the actuator. The velocity is measured at a frequency of 20 kHz in order to provide time-resolved measurements. The moving mechanism go through a fine mesh with 1 $mm \times$ 1 mm spatial discretization, in a parallel plan to the exit nozzle. For each point, the velocity and the reference measurements are done simultaneously on the same time base. To synchronize all the measurements, a conditional approach is employed using the reference sensor trigger in order to have a new time origin. Thanks to the local data synchronization, the 2D velocity field is reconstructed for each time step in a typical period of the sweeping jet actuator. These instantaneous space-solved velocity fields can be animated in time to finally have a spatially-resolved and time-resolved velocity field. To have an efficient characterization in space and time, a nominal point has to be chosen. The amplitude of the velocity peaks has to be strong, and the sweeping frequency steady. Since an inlet pressure of 1 *bar* gives great results in terms of frequency steadiness, this pressure will be retained for the present analysis. This inlet pressure corresponds to a

sweeping frequency of 639 Hz. Fig.6 shows the flowchart of the conditional synchronization procedure. This procedure leads to a 2D space-time resolved velocity field, which allows following the sweeping motion of the jet in time and space.

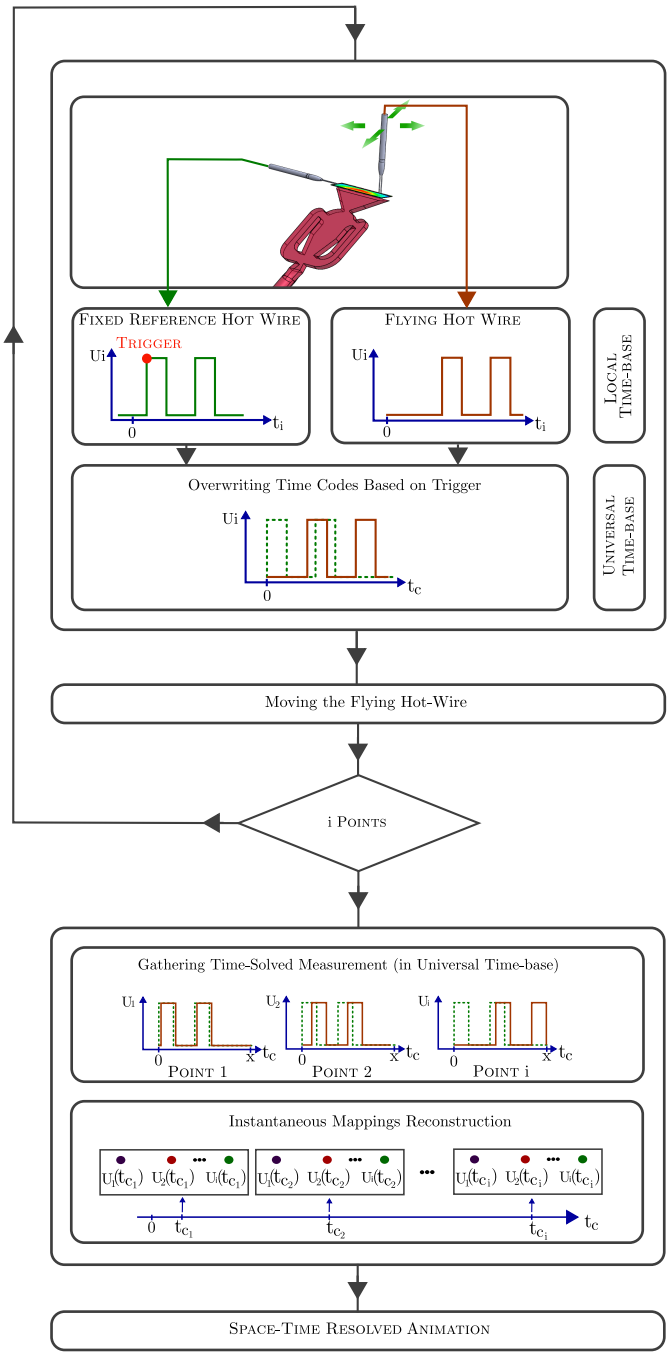

Figure 6 – Hot-wire procedure for the conditional synchronization approach

4. Baseline Flow Field Characterization

This section presents the baseline flow field obtained with the characterization methods stated in section 3, applied to the in-house sweeping jet actuator. These preliminary results are used to improve the understanding of the unsteady flow behavior, while optimizing the experimental setup that will be used for the dynamic analysis of the unsteady flow field (in terms of sensors positioning, sweeping frequency ...).

4.1. Jet Characteristics

The shadowgraph method allows visualizing a refractive index variation created by a density variation. However, the jet velocity has to be high enough to have a refractive index variation that can be captured. The flow visualization is done for various inlet pressure ranging from 0.5 *bars* to 6 *bars*. The main structure of the jet can be quantitatively observed from instantaneous snapshots. Fig.7 is extracted from visualizations with an inlet pressure of 5 *bars*. The shadowgraph in the YZ plan (Fig.7 Left) clearly shows the 45° angle of the jet as expected from the design of the actuator. These indications are used to center the jet in the mesh of the hot-wire scanning. The visualization also highlighted the expansion length of the jet. For this inlet pressure (5 *bars*) the jet is able to reach a distance of $0.8h$ in the 45° plan. The sweeping nature of the jet is demonstrated with the XZ plan shadowgraph measurement (Fig.7 Right). It can be noticed that the jet can potentially interact with the crossflow up to a distance of $0.2h$. Based on these flow observations, the hot-wire sensors positions are adjusted in order to capture the induced flow dynamics.

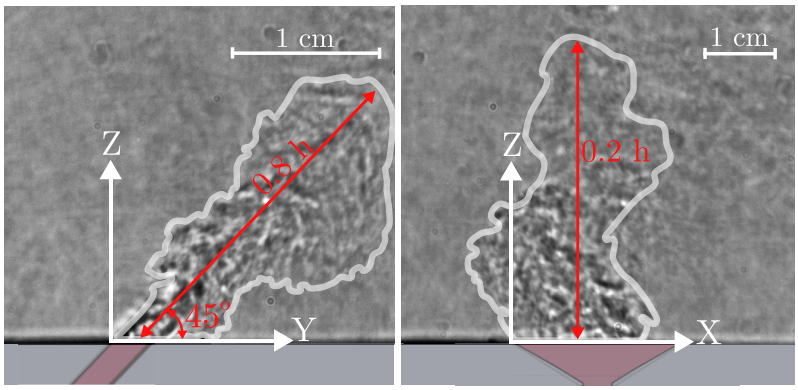

Figure 7 – Instantaneous shadowgraph snapshots

4.2. Mean Flow Characterization

Single-hot-wire measurements are performed in order to characterize the velocity field at the exit nozzle of the actuator. An average flow field is captured (average velocity on 1000 sweeping periods) to visualize the velocity peaks distribution at the exit nozzle. Fig.8 shows the single-hot-wire 2D mapping done for a 25 $mm \times 5$ mm area. In order to avoid perturbations from the interactions between the flow and the sensor, the measurement plan was located at $Z = 1$ mm from the nozzle.

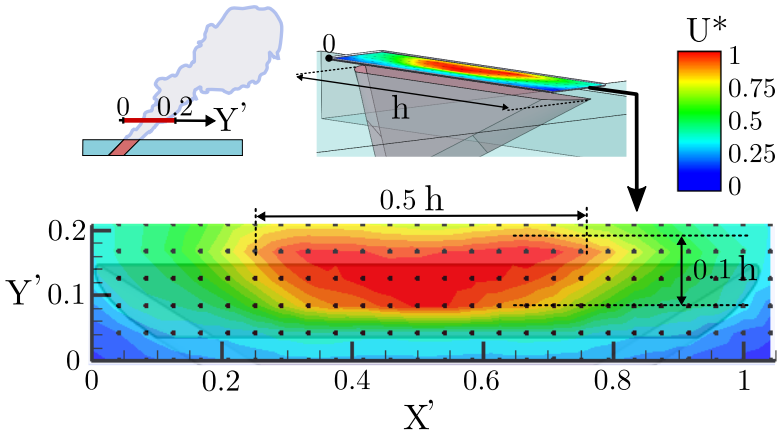

Figure 8 – Single-Wire Hot-Wire 2D Scanning (Time-Averaged)
U^* is defined by the ratio between the average velocity on each point U and the maximum velocity on the whole field U_{MAX}. X^* and Y^* are the dimensionless spatial coordinates using the length of the exit nozzle h. The jet center is determined by the condition $U(x, y) \geq 95\% \times U_{\text{MAX}}$.

In this configuration the flow crosses the measurement plan with a 45° angle in the YZ plan. The single-wire hot-wire sensor is parallel to the X axe. The streamline velocity measured is then a combination of the Y and Z components of the velocity. This configuration was chosen considering that the X velocity of the jet center is weaker than the jet mean velocity (respectively 30 m/s against 81 m/s at 1 bar inlet pressure). The results show that the maximum average velocity is delivered in a crossflow surface of about 40% of the total nozzle surface and is localized at its center. The average jet center is $0.5h$ wide and $0.1h$ thick. The unsteady nature of the jet can be quantified by the RMS (root mean square) profile. Two symetrical peaks are clearly visible and highlight the large fluctuations due to the switching behavior of the jet leading to strong shear layer unsteadiness around $X^* = 0.15$ and $X^* = 0.82$. The RMS velocity data obtained from the hot-wire measurements are nondimensionalized with the local maximum velocity at each position on Fig.9.

Similar behaviors with two RMS peaks were also observed by Koklu and al. [17]). The present results show a maximum turbulent intensity of 104 % for the left peak (at $X^* = 0.15$) and 112 % for the right peak (at $X^* = 0.82$). To focus on the dynamic response of the actuator, measurements are performed with a fixed hot-wire. It is placed in the middle of the exit nozzle, between the two RMS peaks. Fig.10 shows the shape of the raw signal that can be captured in 2 periods of time (here with an inlet-nozzle pressure of 0.5 bar).

At the center of the exit nozzle, the hot-wire captures the double frequency (two jet peaks per period). The jet peaks have silimar shapes and velocities magnitudes independently of the sweeping motion (from right to left or left to right as shown on Fig.10). This method allows to measure the maximum velocity and the frequency response for several inlet pressure (Fig.11 Left). This characterization shows that the actuator has a repeatable behavior up to 4.5 bar. For higher inlet pressures (4.5 bar to 6 bar not shown here), the frequency responses are not steady. This restriction was observed by Gosen and al. [34]. In this

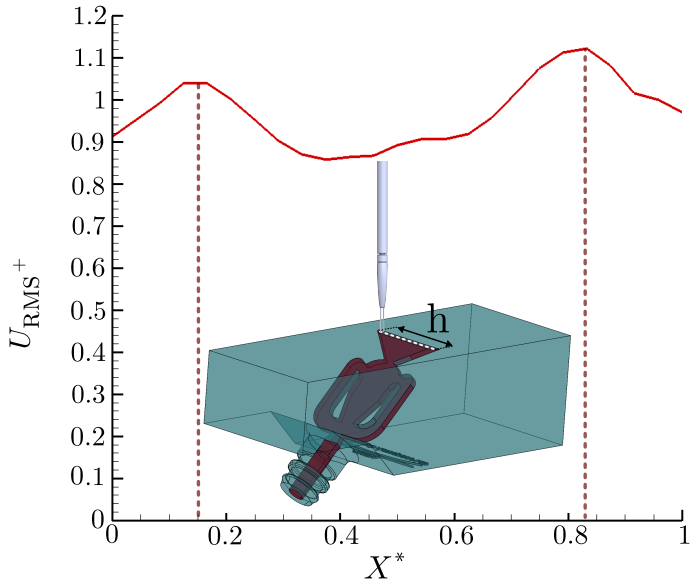

Figure 9 – 1D Single-Hot-Wire Scanning (RMS profils)
$U_{RMS}{}^{+}$ is defined by the ratio between the RMS velocity U_{RMS} and the local time-average velocity U_{MOY}. The spatial coordinates are nondimensionalized with the exit nozzle length h.

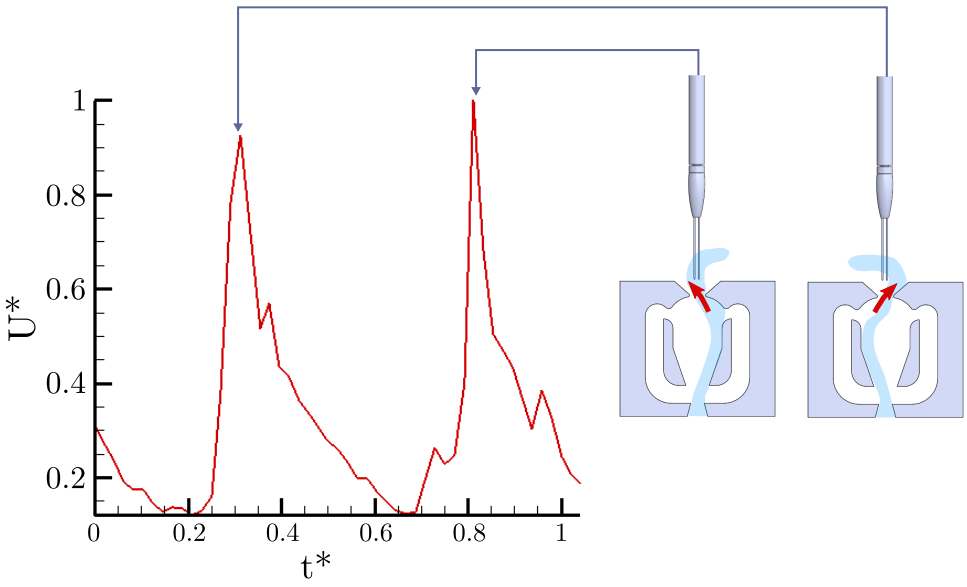

Figure 10 – Single-hot-wire scanning (time-resolved signal - raw experimental data)
With $U^* = U/U_{MAX}$ the velocity nondimensionalized by the maximum velocity in time, and t^* the dimensionless time defined by $t^* = t/T$ with T the sweeping period.

range of pressure the actuator is blowing from 40 $m.s^{-1}$ to 140 $m.s^{-1}$ and is sweeping from 300 Hz to 1 kHz. These ranges are in agreement with previous the researches: among others, Kokul and al. [17] presented a sweeping jet actuator sweeping at 150 Hz and blowing at

100 $m.s^{-1}$. Woszidlo and al. [20] introduced a sweeping jet actuator that can sweep from 500 Hz to 4.5 kHz with a velocity from 10 $m.s^{-1}$ to 450 $m.s^{-1}$. Raman and al. [19] used a miniature fluidic oscillator that reached nearly 3 kHz for an inlet pressure of 3 bar (with a 1.693 $mm \times 0.954$ mm square-wave nozzle). Taking into account the high-pressure loss coefficient induced by the strong geometric variations especially at the output of the device, the range of exit velocity is correlated with isentropic calculations.The Fig.11 Right shows the impact of both a crosswind velocity and the inlet pressure on the sweeping angle. It shows that at a low sweeping frequency and a low actuator velocity, the impact of the crosswind is high (20 m/s crosswind decreases the sweeping angle of 20%). For inlet pressure higher than 1 bar, the crosswind velocity has a lower impact on the sweeping angle (20 m/s crosswind decreases the sweeping angle of only 1%). The inlet pressure decreases the sweeping angle as well (13% losses in sweeping angle for 2.5 bar of inlet pressure increment).

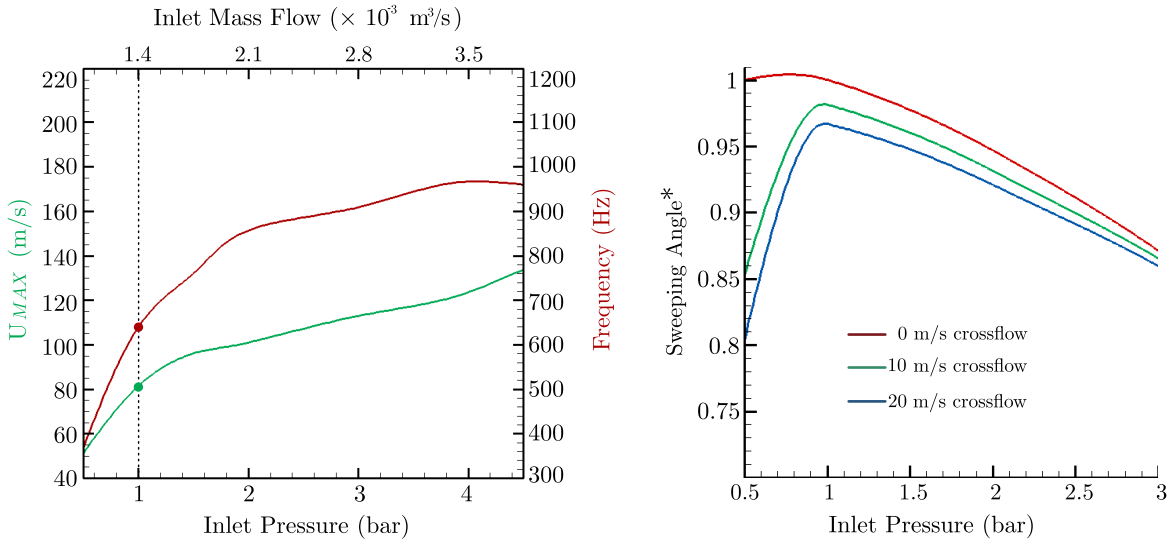

Figure 11 –
LEFT: Actuator Dynamic Response without crossflow
The red curve denotes the frequency response, and the green curve the maximum velocity of the actuator for an inlet pressure varying from 0.5 bar to 4.5 bar. UMAX is the maximum velocity measured on the total acquisition time (4 seconds at 20 kHz).
RIGHT: Parametric Characterization of the Sweeping Angle with crossflow
By defining the jet span as the region where $U_{RMS} > 30$, the sweeping angle can be calculated and the dimensionless sweeping angle is defined by $Sweeping\ Angle^* = SweepingAngle/MaximumSweepingAngle$. These measurements are done for inlet pressure from 0.5 bar to 3 bar and for three crosswind conditions (0 m/s, 10 m/s, and 20 m/s).

To characterize the time dependence of the sweeping jet frequency, two operating points are chosen: one at low sweeping frequency (640 Hz for 1 bar inlet pressure) and one at high sweeping frequency (967 Hz for 4 bar inlet pressure). A Ricker wavelet study is proceeded at these sweeping frequencies. The wavelet is able to analyse the hot-wire signals in time and scale [35] [36]. This process is similar to a sliding Fast Fourier Transform on a time

window. However, the Fourier transformation is not adapted to non-stationary processes. As the time-frequency decomposition method allows to keep the temporal dimension of the spectrum, this method is usually more suitable to describe the time-frequency interaction of such unsteady flows. Continuous wavelet transformation (CWT) is used in the present paper and can be defined as:

$$c(s,t) = \int_0^\infty u(t)\, \tilde{\Psi}_{s,t}(t)\, \mathrm{d}t.$$

The complex conjugaison is denotes by $\tilde{}$, the subscript s and τ denote the scale and the time shaft, and Ψ is the mother wavelet used:

$$\Psi_{s,\tau}(t) = \frac{1}{\sqrt{s}} \left(\frac{t-\tau}{s} \right),$$

with

$$\Psi(t) = \left(1 - t^2\right) e^{-\frac{t^2}{2}}.$$

The scalar product of the wavelet coefficient c is used in order to give information about the unsteady flows.

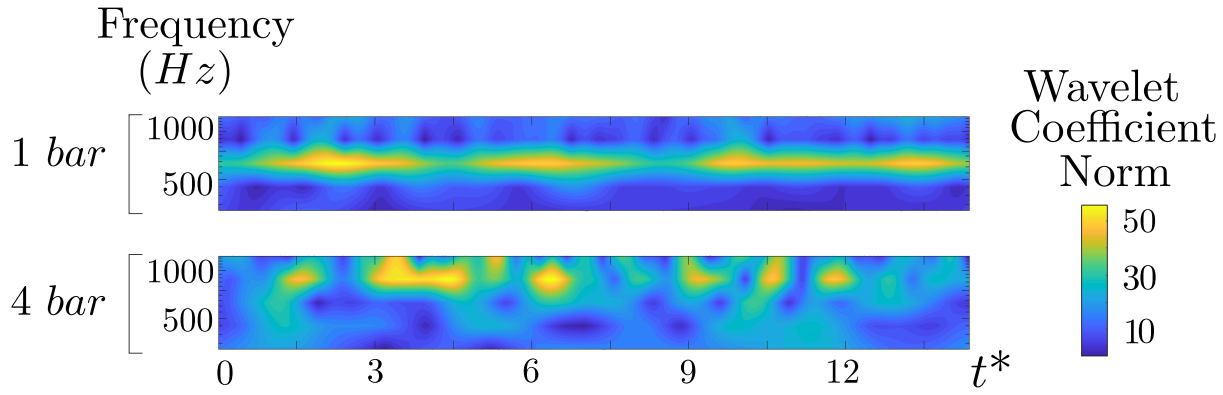

Figure 12 – Frequency steadiness investigation using wavelets
Dimensionless wavelet energy scalogram $\|c(s,\tau)\|^2$ obtained from raw hot-wire data with 4 *bar* inlet presure. The horizontal axis are the time nondimensionalized with the sweeping jet period, and the vertical axis are the frequencies in Hz.

The wavelets shown on Fig.12 indicate that the sweeping frequency is more steady for low velocity and low sweeping frequencies than for high velocity and sweeping frequencies. Indeed, for a 1 *bar* inlet pressure, the sweeping frequency trace has higher amplitudes and is quasi-periodic: the sweeping frequency is almost steady. For a 4 *bar* inlet pressure, the sweeping frequency trace is broader and less intense. The periodicity does not appears as blatantly as for lower inlet pressure: the sweeping frequency becomes gradually unsteady for high inlet pressure.

Based on this global characterization of the sweeping jet actuator response and its jet topology, the experimental setup of the two single-hot-wire can be adjusted and implemented to investigate the dynamic motion of the sweeping jet.

5. Dynamic Analysis of the Unsteady Flow Field

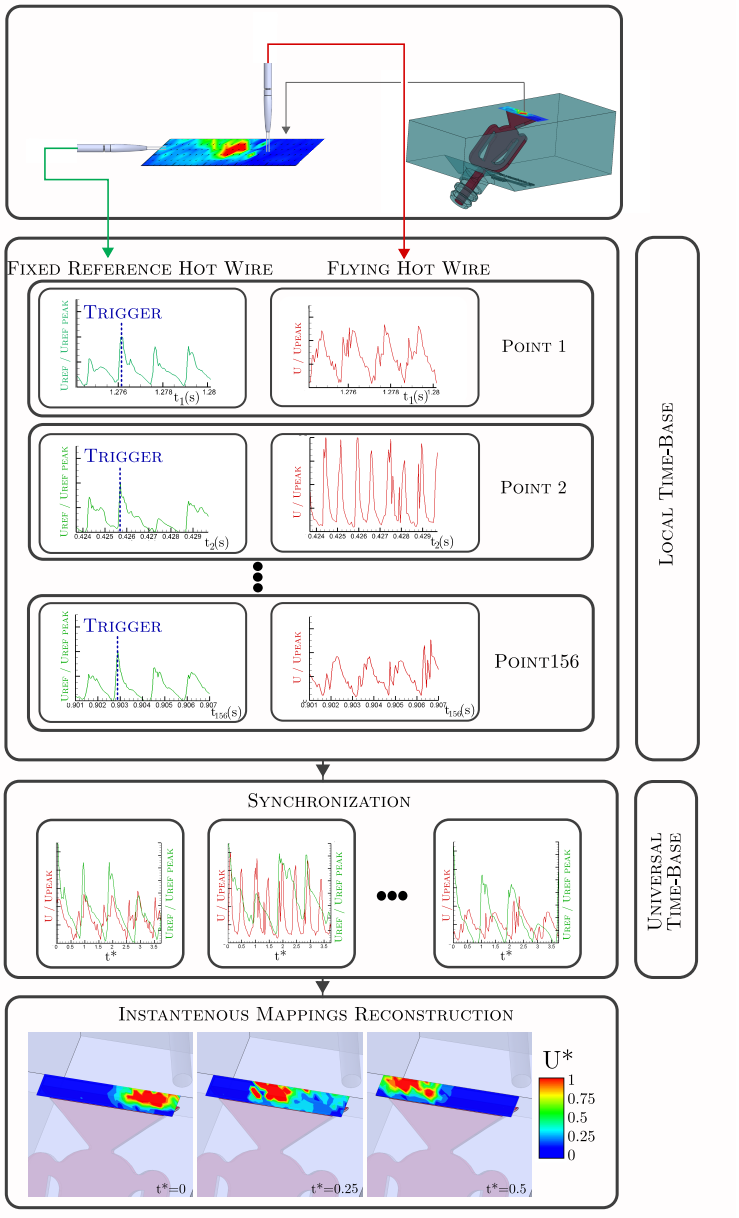

Figure 13 – Space-time resolved mapping: example at 639 Hz For each point, the trigger is localized and the local time-base is replaced by the universal time-base (the new origin corresponding to the trigger peak). The local time-respoved files are then dispatched into 2D space-resolved snapshots for each time step.

The synchronization process described in sub-section 3.3 is now applied to the in-house sweeping jet actuator to characterize its dynamic response using spatially-resolved snapshots. The setup determined in section 4 is used: the inlet pressure is set at 1 bar, which corresponds to a sweeping frequency of 639 Hz. The flying single-hot-wire sensor scans a 25 $mm \times 5$ mm XY plan at $Z = 1$ mm over the exit nozzle. This sensor is traveling with $Z = 1$ mm increments. It stays 3 s per location (1 s waiting for the flow to be established and 2 s of measurements). The synchronization wire is motionless and is located at the left edge of the jet, where it can capture only one velocity peak per sweeping period. The position of this sensor is roughly chosen using the shadowgraph visualizations, and then refined by trial-error. The synchronization trigger is determined on this raw signal with a maximum localization process. To isolate a sweeping period, phase locked averaging method does not give satisfying results: variations in the internal flow conditions contribute to the variations in the instantaneous oscillation frequency which changes randomly. Koklu and al.([17]) quantified this frequency deviation from 10% to 20% around the dominant frequency. This «jittering» makes it difficult to implement a phase averaging post-treatment process. For this reason, the time-resolved mapping is performed on raw data for three sweeping periods on Fig.13. By animating these 2D snapshots in time, the motion of the jet peak at the exit nozzle can be followed. It allows to measure the amplitude and the spreading angle of the jet. This video can be found at the following link: https://vimeo.com/286171518, but Fig.14 shows a set of snapshots extracted from this video.

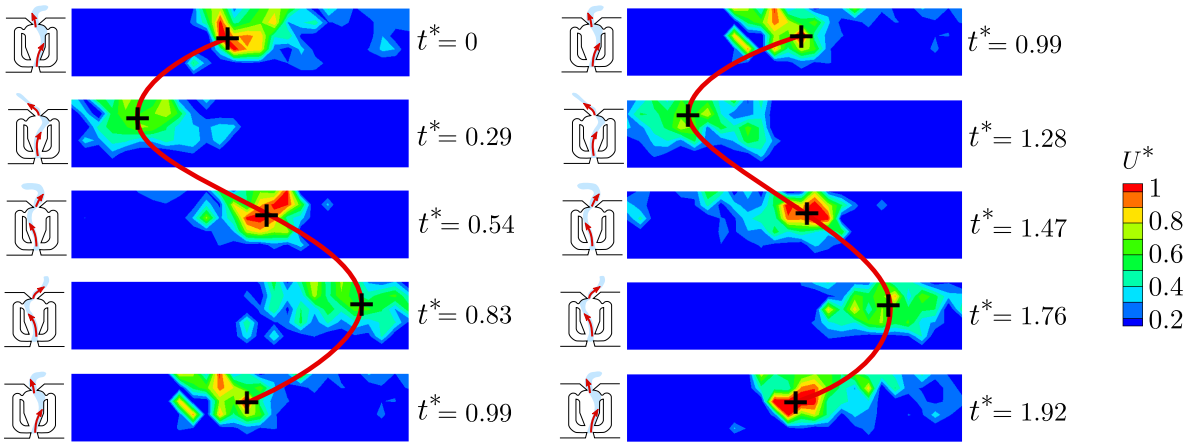

Figure 14 – Instantaneous snapshots data
This set presents some of the instantaneous snapshots. Only ten times instants are chosen, representing the extremum positions of the jet during 2 periods. The time instants t^* are defined by $t^* = t/T$ with T the sweeping period. The velocity magnitude is noted U^* defined by the ratio between the local velocity and the maximum velocity on the whole field U_{MAX}. The cross symbol denotes the jet center, the red curve is the center trajectory.

The jet center is noticed easily on the snapshots, and the wake of its horizontal motions enables to determine whether it comes from the right or from the left. The jet velocity magnitude is higher when the jet is at the center of the exit nozzle than when it is on both

edges. Also, the size of the jet center is bigger. Peaks on both edges of the exit nozzle are quasi-symmetrical. By using all snapshots, the jet center can be followed in time. Fig.15 shows the position reports of the jet center during one period.

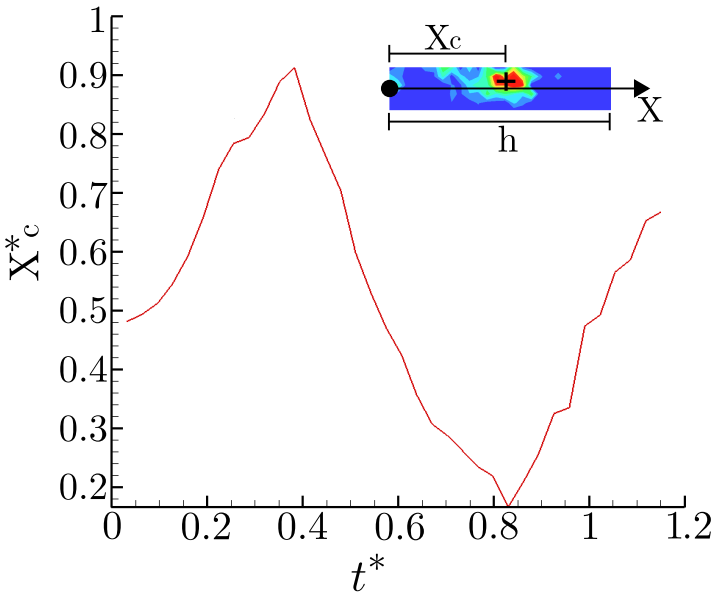

Figure 15 – Jet center position report
for each time instant, the position of the subscript c denotes the position of the jet center. The position is nondimensionalized by the exit nozzle length h, and the time by the period $t^* = t/T$.

Position reports of jet center shows sawtooth periodic signal. In terms of sweeping velocity, this observation shows that the jet center switches position (bi-stable attachment) with a quasi-constant velocity. This horizontal velocity averages $0.3 \times U_{\text{MAX}}$ with maxima at about $0.7 \times U_{\text{MAX}}$. The sweeping process is instantaneous: the jet does not stay on one side or the other. As soon as it reaches one of the extremum positions, the pressure balance in the feedback channels reverses and the jet motion is set. Concerning the amplitude of the sweeping motion, the jet center runs through $0.92 \times h$ along the exit nozzle.

6. Conclusions

This paper presents an experimental methodology to characterize at high frequency a sweeping jet actuator in space and time. In the first part of the paper, the in-house sweeping jet actuator is described. Its design is based on the literature, however, the global size is extended to be compatible with a prospective experiment. The actuator is manufactured at ONERA Lille. The second part of this paper presents the metrology equipment used to characterize the sweeping jet flow, and the double single-hot-wire procedure for the conditional synchronization approach is introduced. This novel approach gives a space-time resolved characterization at high sweeping frequency using two synchronized hot-wire sensors: one used as a reference signal and the other used as a flying sensor. In the third part of the paper, the base flow of the sweeping jet is characterized at the exit nozzle by shadowgraph visualizations. Thanks to these visualizations, the jet topology can be defined. Consequently, the position of the sensors can be adjusted for the measurements. Single-hot-wire measurements are then performed to define the dynamic response of the actuator and be able to link the inlet pressure with the velocity response of the sweeping frequency. This simple hot-wire characterization shows a sweeping jet actuator that is in accordance with the literature in terms of frequency range and behavior. Thanks to these measurements a nominal inlet pressure is chosen for the conditional approach characterization. In the fourth and last part of the paper, the conditional synchronization approach is used to characterize the dynamic response of the sweeping jet actuator at the nominal point chosen, which corresponds to a sweeping frequency of 639 Hz. The flying hot-wire sensor covers a 125 mm^2 2D mapping at the exit nozzle plan with a time resolution of 20 kHz and a spacial resolution of 1 mm. This characterization is well suited for sweeping jets because there is no electronic input or output signal (unlike pulsed or synthetic jet, for which there is an input signal that can be used as a trigger). Further investigations will be done with this actuator to study the interaction between the sweeping jet and a crossflow (turbulent boundary layer). The same characterization process will be applied with hot-wire scanning in a volumetric mesh. For this application the present method has some limitations. The synchronization hot wire is quite intrusive and disturbs the flow downwind. Moreover, the sweep angle being a function of the cross-flow strength, the synchronization sensor will not necessarily be in the correct location and thus will not capture the jet peak for each period. Therefore, the reference hot-wire sensor will be replaced by a pressure sensor in one of the feedback channels for future research.

7. Acknowledgements

The present work has been supported by Campus International pour la Sécurité et l'Intermodalité des Transports, la Région Hauts-de-France, l'Union Européenne, la Direction de la Recherche, Enseignement Supérieur, Santé et Technologies de l'Information et de la Communication and le Centre National de la Recherche Scientifique. The authors gratefully acknowledge the support of these institutions.

[1] Cattafesta L.N., Sheplak M., Actuators for Active Flow Control, Annual Review of Fluid Mechanics (2011).
[2] Ternoy F., Dandois J., David F., Pruvost M., Overview of ONERA Actuators for Active Flow Control, Aerospace Lab, p. 1-14 (2013).
[3] Chovet C., Lippert M., Keirsbulck L., Foucaut J.-M., Dynamic characterization of piezoelectric microblowers for separation flow control., Sensors and Actuators A Physical, (2016).
[4] Naik N., Courcimault C., Hunter H., Berg J., Lee J., Naeli K., Wright T., Allen M., Brand O., Glezer O., King W., Microfluidics for generation and characterization of liquid and gaseous micro and nanojets, Sensors and Actuators A 134 119?127 (2007).
[5] Housera N.M., Gimenob L., Hansona R.E., Goldhawkc T., Simpsonc T., Lavoiea P., Microfabrication of dielectric barrier discharge plasma actuators for flow control, Sensors and Actuators A 201 101:104 (2013).
[6] Kral L.D., Active Flow Control Technology, ASME Fluids Engineering Division Technical Brief (2000).
[7] Warren R.W., Some Paremeters Affecting the Design of Bistable Fluid Amplifiers, Fluid Jet Control Devices, ASME (1962).
[8] Vietz H., Flip-Flop jet Nozzle, AIAA Journal Vol.13 NO.10 (1975).
[9] Vollmer J., Hein H., Menz W., Walter F., Bistable fluidic elements in LIGA technique for flow control in fluidic microactuators, Sensors and Actuators A 43 33C-334(1994).
[10] Theofilis V., Role of instability theory in flow control (2009).
[11] Sattarzadeh S.S., Fransson J.H.M., Experimental investigation on the steady and unsteady disturbances in a flat plate boundary layer, PHYSICS OF FLUIDS 26 124103 (2014).
[12] Gallas Q., Pruvost M., Characterization of Fluidic Micro-Actuators, VKI Workshop on safety and control valves (2015).
[13] Ternoy F., Dandois J., Eglinger E., Delva J., Overview of ONERA Fluidic Actuators in Aerodynamics, In Proceedings of the Actuator, Bremen, Germany (2018)
[14] Poisson-Quinton P., Recherches théoriques et expérimentales sur le contrôle des couches limites, Londres Congress of Applied Mechanics (1948).
[15] Poisson-Quinton P, Lepage L., Survey of French Reasearch on the Control of Boundary Layer and Circulation, s.l. Boundary Layer and Flow Control (1961).
[16] Horne W.C., Burnside N.J., Acoustic Study of a Sweeping Jet Actuator for Active Flow Control Applications, 22nd AIAA/CEAS Aeroacoustics Conference (2016).
[17] Koklu M., Melton L.P., Sweeping Jet Actuator in a Quiescent Environment, AIAA 43rd Fluid Dynamics Conference (2013).
[18] Koklu M., Effect of a Coanda Extension on the Performance of a Sweeping-Jet Actuator, AIAA Journal Vol.54 No.3 pp.1131-1134 (2016).
[19] Raman G., Raghu S., Cavity Resonance Suppression Using Miniature Fluidic Oscillators, AIAA Journal Vol.42 No.12 pp.2608-2612 (2004).
[20] Woszidlo R., Nawroth H., Parametric Study of Sweeping Jet Actuators for Separation Control, 5th AIAA Flow Control Conference (2010).
[21] Peters C.J., Miles R.B., Femtosecond Laser Tagging Characterization of a Sweeping Jet Actuator Operating in the Compressible Regime, 32nd AIAA Aerodynamic Measurement Technology and Ground Testing Conference (2016).
[22] Ostermann F., Godbersen P., Woszidlo R., Nayeri C.N., Paschereit C.O., Sweeping Jet from a Fluidic Oscillator in Crossflow, Phys. Rev. Fluids 2, 090512 (2017).
[23] Hirsch D.G., An Experimental and theoretical study of active flow control, Ph.D. Thesis (2017).
[24] Ostermann F., Woszidlo R., Nayeri C.N., Paschereit C.O., Phase-Averaging Methods for the Natural Flowfield of a Fluidic Oscillator, AIAA Journal vol.53 NO.8 (2015).
[25] Sieber M., Ostermann F., Woszidlo R., Oberleithner K., and Paschereit C., Lagrangian Coherent Structure in the Flow Field of a Fluidic Oscillator, Phys. Rev. Fluids, 1, p. 050509 (2016).
[26] Arnault A., Dandois J., Numerical study of an isolated sweeping jet, rapport de stage ONERA (2013).
[27] Duda B., Unsteady Flow Simulation of a Sweeping Jet Actuator, 54th AIAA Aerospace Sciences Meeting

(2016).
[28] Kara K., Numerical Study of Internal Flow Structures in a Sweeping Jet Actuator, 33rd AIAA Applied Aerodynamics Conference (2015).
[29] Seele R., Graff E., Lin J., Wygnanski I., Performance Enhancement of a Vertical Tail Model with Sweeping Jet Actuators, 51st AIAA Aerospace Sciences Meeting (2013).
[30] Dandois J., Active flow control for Low and High-Speed Flows, Mémoire d'Habilitation a diriger des recherches, UPMC-ONERA (2017).
[31] Tewes P., Taubert L., Wygnanski I., On The Use of Sweeping Jets to Augment the Lift of a λ-Wing, 28th AIAA Applied Aerodynamics Conference (2010).
[32] Seele R, Graff E, Gharib M, Taubert L, Lin J, Wygnansi I, Improving Rudder Effectiveness with Sweeping Jet Actuators, 6th AIAA Flow Control Conference (2012).
[33] Graff E., Seele R., Lin J., Wygnanski I., Sweeping Jet Actuators: A New Design Tool for High Lift Generation, Innovative Control Effectors for Military Vehicles (2013).
[34] Gosen F., Ostermann F., Woszidlo R., Nayeri C., Paschereit C.O., Experimental Investigation of Compressibility Effects in a Fluidic Oscillator, 53rd AIAA Aerospace Sciences Meeting (2015).
[35] Farge M., Schneider K., Wavelets: application to turbulence, Centre for Fusion Space and Astrophysics Courses (2005).
[36] M. L. S. Indrusiak M.L.S., Kozakevicius A.J., Möller S.V., Wavelet Analysis Considerations for Experimental Nonstationary Flow Phenomena, Thermal Engineering Vol.15 No.1 p. 67-76 (2016).

8. Biographies

Célestin Ott was born in France in 1993. He received his Dipl.-Ing. in the field of fluid dynamics and his Master in Buisness and Administration in 2016 in Valenciennes at the engineering high school Ensiame and the Institute of Business Administration Iae. He is currently a Ph.D. candidate since 2016 until now at the Onera, the French Aerospace Lab in Lille and at the Lamih laboratory from the university of Valenciennes. His research interests cover experimental fluid mechanics and active flow control.

Quentin Gallas was born in France in 1977. A graduate engineer from Politech'Lyon in 2001, he received his master's degree in 2002 and his PhD in 2005 at the University of Florida (USA). Back to France, he joined the Renault group where he spent 9 years in the field of aerodynamics, using both experimental and numerical tools. In 2014 he joined Onera, the French Aerospace Lab, in the Aerodynamics, Aeroelasticity, Acoustics Department in Lille center. He was first in charge of the "Physics of Fluids" activities, and then took in charge the Experimental and Flight Limit unit in 2017 and became the Head of the unit. Since 2018, he is also part of the Laboratory of Fluid Mechanics of Lille (LMFL), where he is in charge of the scientific thematic "Measure and Data analysis" in the laboratory. His areas of study and research cover flow control technologies, development of experimental methodologies and metrology in air and water, and terrestrial and naval aerology.

Jérôme Delva was born in France in 1986. He received his Dipl.-Ing. from the Institut Catholique d'Art et Métiers (ICAM). He is currently an engineer at the Experimental and Flight Limit unit in Onera Lille. His work consist mainly in the experimental characterization of fluidic actuators.

Marc Lippert was born in France, in 1970. He received his Ph.D. degree, in 1999, at the laboratory Iemn-Doae from University of Valenciennes, for his work in the development of a piezoelectric thin film of ZnO. He is currently an engineer at the Mechanical Engineering Department in LAMIH laboratory from the University of Valenciennes. His current research is based on specified techniques of characterization of fluid mechanics.

Laurent Keirsbulck was born in France in 1975. He received his Dipl.-Ing. and doctorate degrees in mechanical engineering from the University of Valenciennes in 1998 and 2000, respectively. Since 2002, he was a research assistant at the LAMIH of which he is the mechanical department Deputy Director. He has worked on several research fields including wall turbulence and flow control. One of his main fields of research focuses on the feedback separation flow control.